CRITICAL REVIEW

Friction drilling: a review

Alexander Eliseev [1] · Evgeny Kolubaev [1]

Abstract

Friction drilling is one of the most promising methods for hole making in thin sheets of conventional structural alloy materials (aluminum, steel, copper, titanium, etc.) and novel polymer composites. Despite almost a hundred year history of studying friction drilling, it is still highly relevant and is actively developed. The aim of the present review is to cover as fully as possible all aspects of this technology. The paper analyzes the advantages and disadvantages of friction drilling, discusses the influence of technological parameters on the drilled hole quality. The technological parameters considered are not only the feed rate and spindle speed, but also the tool configuration. The quality of the holes refers to their strength, inner surface hardness, hole geometry and roughness, bushing geometry, and so on; therefore, they are also analyzed. From a fundamental point of view, frictional drilling is interesting in that it causes structural changes in the material as a result of severe plastic deformation, which is discussed in a separate section. Approaches for the process modeling are considered which quite accurately predict the material behavior. A technically more advanced technology of a new generation is discussed, namely flow drill screwdriving. A general conclusion is that despite the widespread use of friction drilling, including by well-known engineering companies, the technology continues to develop with regard to the changing needs of the industry and the market and strengthens its position in the industry.

1 Introduction

The current trend for energy saving makes it an urgent mechanical engineering problem to reduce the weight of structures. This task is successfully accomplished through the use of light and high-strength materials for the production of critical structures. Moreover, the thickness of sheet materials is significantly reduced, making difficult their thread fastening due to the impossibility to form a sufficient number of thread turns in a thin sheet. The use of spot welding for the joining of thin sheet materials often proves to be inefficient. Spot friction stir welding has a great potential, but it is suitable only for permanent joining, which is not always required. Often, engineering structures are manufactured using special fittings, but it complicates the technology and increases the cost of production.

A more productive technology in this respect is friction drilling, which allows making holes in thin sheet materials with bushings for thread forming. In friction drilling, a rotating conical non-consumable hard alloy tool comes into contact with the workpiece, heats the workpiece material to a plastic state due to the frictional force, penetrates the workpiece due to the axial force, forming a hole and bushing, and then leaves the hole in the opposite direction (Fig. 1). The process temperature in a well-chosen mode does not exceed 0.85 T_m [1] and hence deformation occurs in the solid phase.

The following technological features of friction drilling make it advantageous over conventional drilling with the use of fittings and over other sheet joining techniques:

- bushing formation for thread forming immediately during drilling;
- hardening of the bushing material and, consequently, high thread strength;
- no need to use cleaning and lubricating agents, which makes the process more technological and environmentally friendly;
- no chips, i.e., material saving;
- high rate and efficiency of the process;

✉ Alexander Eliseev
alan@ispms.ru

[1] Institute of Strength Physics and Materials Science of Siberian Branch of Russian Academy of Sciences, Tomsk, Russian Federation

Fig. 1 Steps of the friction drilling process [2]
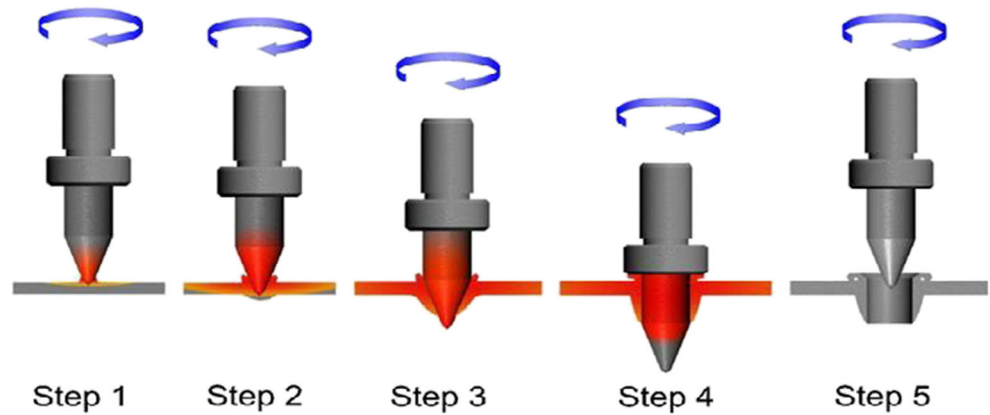
- high quality of holes, with low roughness and high accuracy;
- high volume production capability.

The friction drilling process is also more environmentally friendly than conventional drilling techniques as it consumes less power [3] (Fig. 2). In some categories, the impact of friction drilling on the environment is orders of magnitude less.

The limitations of the technique include the fact that high-quality holes cannot be formed by manual drilling due to the difficulty of maintaining a constant load or feed rate; the technology requires automatic equipment. Another fact is that the process is very sensitive to material, tool, and technological mode, which complicates the selection of these parameters and the optimization of friction drilling [4].

According to the FlowDrill company manual [5], the friction drilling technology was invented by Jan-Claude de Vallière in 1923 in France. This information is widespread

among researchers, but it is not confirmed. The earliest recorded mention of a similar method for making holes in pipes is contained in a 1933 patent issued to W.L. Enghauser [6]. The patent proposes a two-step scheme: (1) a hole is drilled by the conventional method with the aim of marking the hole place and easier formation of a flange, and (2) a flange is formed by a rotating swaging tool.

A one-step process similar to modern technology was described in a 1957 patent issued to A. Leroy [7], who proposed to form holes with flanges in pipes and sheet materials in one step using a rotating tool shaped as an elongated pyramid. The tool configuration closest to the currently used one was proposed in a 1974 patent by J.A. van Geffen [8]. Commercial success of the technology was achieved after the improvement described in 1982–1984 patents by A.J. Hoogenboom [9], G.J. Dekkers [10], and G.D. Head, Jr et al. [11].

Despite a nearly century-long history of friction drilling, it is still a new technology. Its development actually began in the 1970s. That is why there is no established terminology of the

Fig. 2 Environmental impact of various drilling techniques [3]
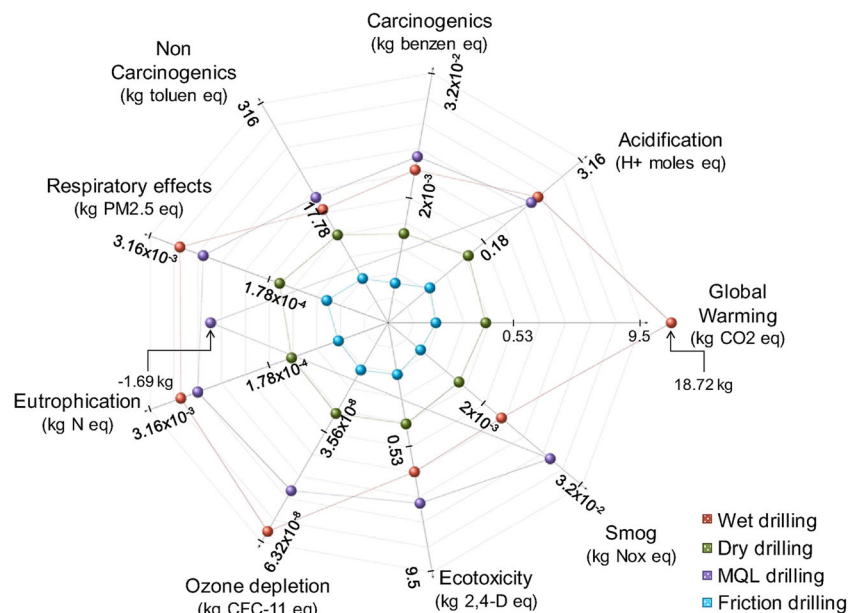
process, both in research and in industry. Friction drilling is also called flow drilling, form drilling, thermal drilling, plastic drilling, thermoplastic drilling, thermomechanical drilling, chipless drilling, or friction stir drilling. The main reason for its slow development at the beginning of the twentieth century is the lack of a sufficiently resistant material for the manufacture of tools. The widespread adoption of numerically controlled machines promoted the introduction of the technology into industry. Today, friction drilling is used by many production companies, e.g., Ford, Voestalpine, and Gestamp for the production of cars, various tanks, accessories, and the construction of bridges, roads, and buildings.

In view of extensive industrial applications, friction drilling is also a subject of the interest for researchers. The number of research papers and reviews in this area increases exponentially, e.g., [12–14]. Here we seek to highlight as completely as possible all aspects of friction drilling investigated to date. The search for publications used the capabilities of the ScienceDirect platform, the ResearchGate social network, and the Google search engine. The search was performed using different variations of the technology name. The reference lists of already found documents were also examined. Patent searches were performed using the INPI patent database, EPO database, and Google Patents.

2 Process technology

The efficiency of the friction drilling process directly depends on a set of initial conditions: physical properties of the workpiece and tool materials and their geometry, spindle speed, tool feed rate or thrust force, the presence or absence of lubrication.

2.1 Tool

The friction drilling tool is studied in terms of its durability and the quality of drilled holes. The most common shape of the tool used today was proposed in a 1984 patent by Hoogenboom [9] (Fig. 3). The tool is a pyramid with rounded equilateral triangle or square cross-section. This configuration was invented in order to reduce tool wear in comparison with previously proposed cylindrical tools.

Most often, the tools are made of tungsten carbide and are cemented or covered by other coatings to increase their lives. For example, Kerkhofs et al. [15] deposited PVD (Ti,Al)N coatings onto cemented carbide tools with rounded triangular cross-section. The life of the coated tools used for friction drilling of austenitic stainless steel with a ZnS-based lubricant increased from 5000–15000 to 100000–160000 bushed holes. Modern friction drilling tools are more durable than conventional twist drills [16]. Tools are also made of H13 steel. For example, in [17], coatings on this steel were compared when

drilling AZ31B magnesium alloy. It was found that PVD TiN coating (physical vapor deposition) keeps tool conicity better than plasma nitriding and liquid nitriding. The wear characteristics of tungsten carbide tools in friction drilling of low carbon steel were investigated by Mutalib et al. [18]. The authors revealed several types of tool wear in friction drilling, such as adhesive, abrasive, and oxidative wear.

The measured tool profile after 200, 400, 600, 800, and 1000 holes showed that only the conical tool parts are worn out due to the high axial force at the initial stages of drilling. The tool mass was reduced by 3.7% after 1000 holes. However, the diameter of the drilled holes decreased slightly with tool wear because the diameter of the cylindrical tool part remained almost unchanged. A similar tool used for the drilling of 11000 holes in low-carbon steel AISI 1015 also generally maintained its shape during wear. The most severe wear was observed in the center, where the cone angle changed (Fig. 4).

Ku et al. [20] used friction drilling tools with different cone angles θ (30–60°) and different friction contact area ratios (FCAR = 50–100%), as shown in Fig. 5. The effect of these parameters on the bushing length was studied by a variational analysis with regard to the influence of the feed rate and spindle speed. The analysis showed that the FCAR has the greatest influence on the bushing length: the smaller the area, the greater the bushing length, all other things being equal. From the viewpoint of the torque-to-load ratio, a tool with 50% FCAR is the most efficient for drilling AISI 304 stainless steel [21]. In general, tools with reduced FCAR provide better holes and therefore they are more common. Increasing tool diameter leads to an increase in the hole diameter error, as shown for AISI 304 steel by El-Bahloul et al. [22].

The torque and axial force are also strongly affected by the cone angle. With increasing cone angle, the torque decreases and the axial force increases [23]. As was shown in a modeling study of friction drilling [24], the cone angle increase to 90° leads to an increase in torque, axial force, and temperature, but the drilling time is almost halved.

One of the important factors in tool wear in industrial applications of the technology is high temperature. Tool heating can cause structural changes in the tool material and increased oxidation. For better production efficiency, it is reasonable to drill holes in minimum time intervals, but then the tool does not have time to cool down. This problem is solved using various tool holders with cooling disks. Despite the different design solutions, all holders are generally constructed based on the same principle of air pumping into the drilling zone.

2.2 Technological mode

There are two types of friction drilling modes: soft mode when drilling is carried out with a constant load on the tool, and hard mode with a constant feed rate. In soft mode, the material

Fig. 3 Schematic view of the friction drilling tool: 1 — rotating spindle, 2 — tapered center point, 3 — first conical part, 4 — second prismatic part, 5 — collar, 6 — shoulder, 7 — shaft [9]
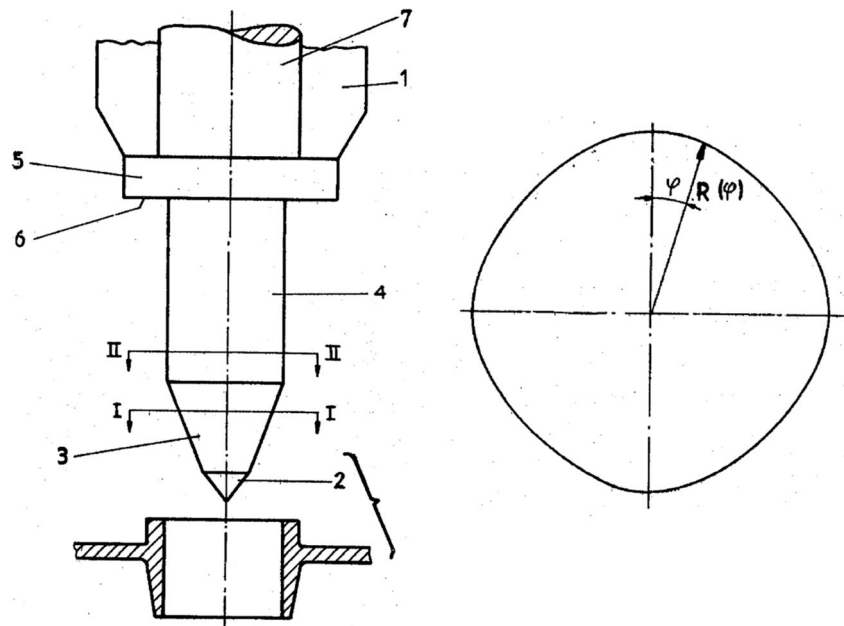
flows smoothly and the workpiece is not damaged due to the absence of overloads. The time variation curve of the feed rate in soft mode is non-linear. This non-linearity is caused by the natural mechanisms of material flow under the tool. The disadvantage of the soft mode is either an insufficient load for the necessary heating, or vice versa overheating due to too high load. The given mode is not suitable for mass production.

Hard mode is more convenient for mass production with the use of numerically controlled machines. Its main drawback is that if the tool is plunged into the workpiece without taking into account the response of the material, there may be an uncontrolled increase in the axial force resulting in damage to the workpiece or the tool. A possible solution to this problem is to set a different feed rate for each stage of the drilling process.

The characteristic variation curves of the torque and axial force in the hard-mode drilling of sheet materials are illustrated in Fig. 6 [25]. The maximum axial force is reached at the beginning of the tool–workpiece engagement and then

decreases due to heating. The axial force decrease is non-linear because the tool geometry changes along the length. The highest temperature is reached at the end of phase V [26], after which the axial force sharply increases again due to the expansion of the upper bushing by the tool shoulders. In doing so, the torque continuously increases from the beginning of drilling with increasing tool–workpiece contact area. When the lower surface is ruptured by the tool, the torque sharply decreases as the cylindrical part of the tool is engaged with the workpiece and then increases again when the shoulders come into contact with the upper bushing part.

In the case of constant spindle speed and increasing feed rate, the load on the tool increases. With constant feed rate but increasing spindle speed, the axial force decreases. The maximum temperatures reached in drilling aluminum, brass, and stainless steel sheets of 1.5-mm thickness with the spindle speed 3500 rpm were respectively 164°C, 252°C, and 468°C [27]. In this work, the temperature was measured with an infrared thermometer. The accuracy of such devices is up to

Fig. 4 Measured profiles of the friction drilling tool after 0–11000 holes [19]
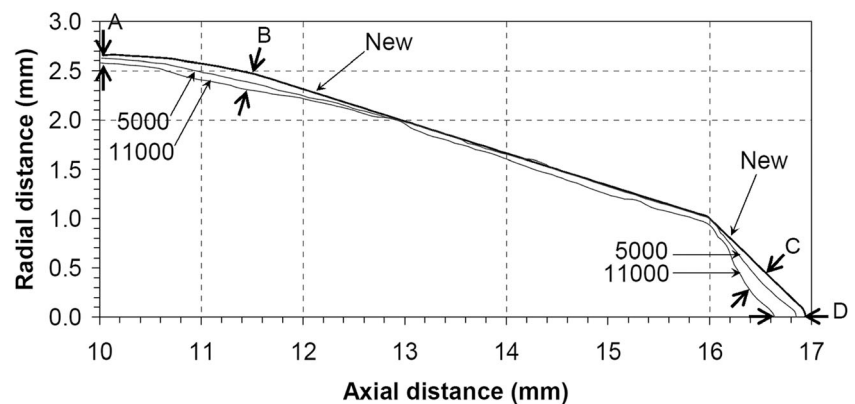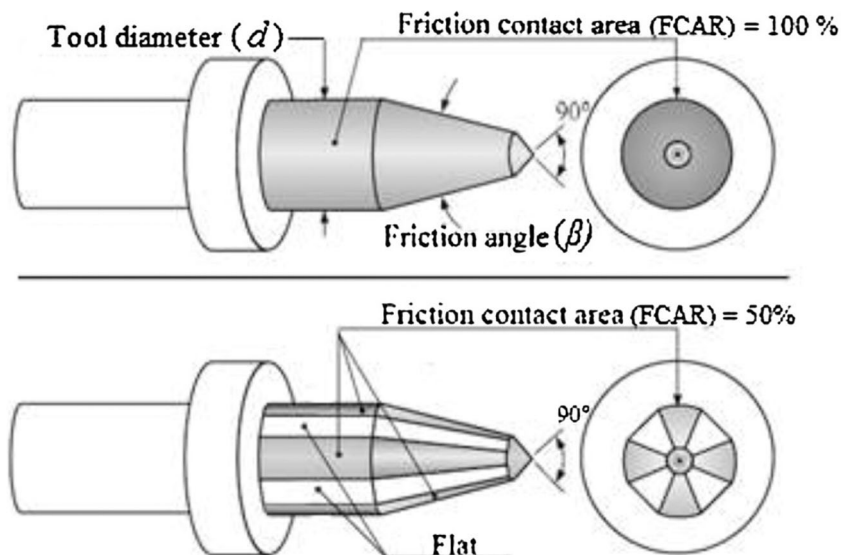
Fig. 5 Front and side views of thermal friction drills for two different friction contact area ratios (FCARs) [21]

1 °C. However, it should be kept in mind that when using non-contact methods, any measurement will only show the surface temperature. In this case, the maximal temperature can be registered at the tool-material interface, where friction occurs directly. The resulting value will actually be the average temperature in that area, since the measurement spot can be up to several millimeters in size. Nevertheless, this method allows temperature estimates to be made when significant deviations are observed. In general, temperature measurement in any such process is extremely difficult. Non-contact methods measure only the surface temperature. Thermocouples allow to obtain only the average temperature of a material's macrovolume.

Demir and Ozek [28] studied friction drilling of aluminum alloys 1050, 5083, 6061, and 7075 with feed rates of 25–100 mm/min and spindle speeds of 1200–4200 rpm. It was shown that the process temperature value correlates with the shear strength of the material. The highest temperature of 241°C was achieved in AA5053 alloy with 25 mm/min feed rate and 4200 rpm spindle speed. The lowest temperature of 87°C was observed for AA1050 with 100 mm/min feed rate and 1200 rpm spindle speed. With constant feed rate and increasing spindle speed, the temperature in all alloys increased monotonically. With increasing feed rate and constant spindle speed, on the contrary, the temperature decreased due to the shorter contact time of the tool with the material. In the

Fig. 6 Variation of the axial force and torque during friction drilling [25]
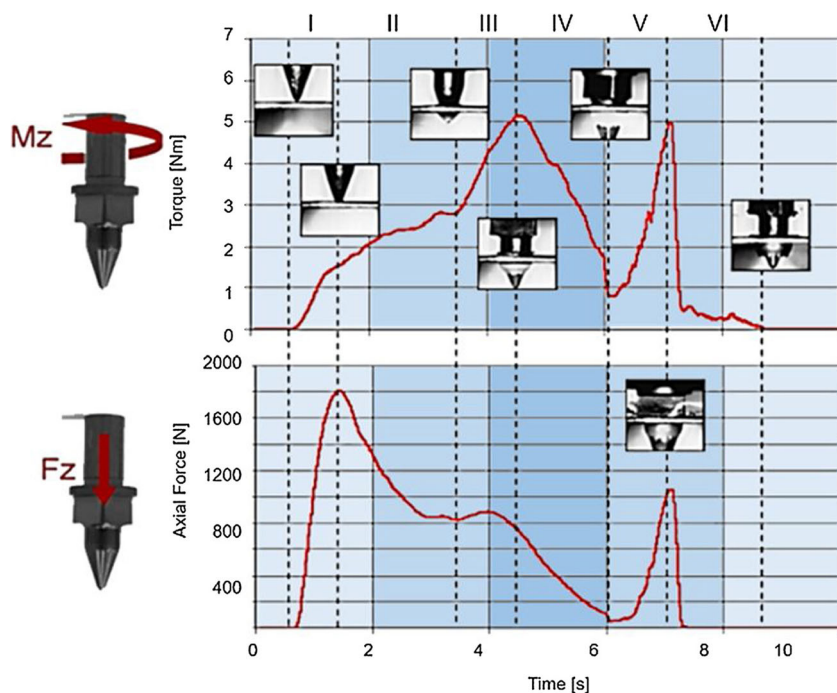
case of low spindle speed and a large thickness of the work-piece, friction drilling cannot be completed due to a lack of thermal energy; the tool is only pressed through the workpiece material.

An important process parameter is the sheet thickness to tool radius ratio. The greater this ratio, the higher the torque and the axial force on the tool, all other things being equal [29]. Variational analysis and the Taguchi method showed that the most optimal value of this ratio in terms of the balance between axial force and torque is 0.11. However, if this ratio is reduced, the roughness of the walls increases, which reduces the hole quality. The larger the diameter of the hole, the more material is affected. Material from the central portion is affected the most. Also, increasing this ratio can cause the formation of petals. Thus, a balance must be maintained.

Krasauskas [26] studied the influence of the drilling modes, material, and its thickness on the drilling force and torque on the tool for hot rolled S235 steel (2.5-mm thick), AISI 4301 stainless steel (1.5 and 2 mm), and Al 5652 aluminum alloy (1.5 mm). The study was carried out within the spindle speed range 2000–3000 rpm and the feed rate range 60–140 mm/min. It was shown that a higher spindle speed corresponds to a lower drilling force due to higher heating, and the feed rate is directly proportional to the axial force. Statistical analysis of the drilling force data showed that the axial force is most strongly affected by the sheet thickness, feed rate, and yield strength.

According to Rao et al. [30], the greatest influence on the material deformation during friction drilling is produced by the tool feed rate (in comparison with the spindle speed, material, and tool cone angle). The hole surface roughness is most affected by the spindle speed: the higher the speed, the lower the roughness [2]. Dogru et al. [31], on the contrary, showed based on empirical data and variational analysis that the feed rate contributes more to the roughness: the higher the feed rate, the greater the roughness. This contradiction can be explained by the fact that Boopathi conducted research on 2024 aluminum alloy, while Dogru studied AISI 1010 steel. Nevertheless, the spindle speed has a significant effect on the hole surface roughness, as shown by Pantawane and Ahuja [32] for a similar AISI 1015 steel. As the spindle speed increases, the temperature of the friction surface rises, facilitating the material plastic flow. According to [31], the second and third most important inversely proportional contributions to the roughness are the tool cone angle and the spindle speed, respectively. The feed rate has the most pronounced directly proportional effect on the temperature.

Upon reaching a certain threshold, the increasing feed rate, on the contrary, causes an increase in the hole surface roughness, which can be attributed to the lack of time required for material heating [33]. In general, friction drilling of single non-ferrous and steel alloy sheets is currently not a technological problem, in contrast to the drilling of titanium alloys,

sandwiches, and end drilling. As shown by Biermann et al. [34], friction drilling can be applied for making holes in the ends of sheet materials, but this requires preheating the tool. When drilling an AlSi10Mg alloy profile of 6-mm thickness, the best quality bores were produced with tool preheating to 200°C. In the case of overheating or underheating, the bore walls were damaged or their shape was distorted (Fig. 7). In so doing, the preheating temperature slightly affected the axial force and torque on the tool.

Dehghan et al. [35] carried out friction drilling of a 3-mm-thick titanium alloy Ti-6Al-4V using a tungsten carbide tool. The spindle speed varied in the range of 1500–5500 rpm and the feed rate ranged from 65 to 145 mm/min. The best holes in terms of the bushing geometry were obtained in the modes with lower frequency and feed rate. The tool wear was the lowest under the same conditions. With the maximum feed rate, the tool was broken after the first drilling operation. From the viewpoint of maintaining a rounded shape, the quality of friction-drilled holes is, on the contrary, directly proportional to the spindle speed. This was shown by Somasundaram and Boopathy [36] in a study of drilling aluminum silicon carbide metal matrix composite. An increase in the proportion of reinforcing SiC particles negatively affected the quality of the holes.

In general, each material has a specific range of acceptable parameters. As shown in [37], high-quality joints can be obtained by flow drill screwdriving at different parameter ratios. In this sense, friction drilling, flow drill screwdriving, and friction stir welding are very similar. It is known [38], for example, that the range of permissible parameters for friction stir welding of different aluminum alloys can vary greatly.

Despite there are recommendations and extensive data on the influence of technological parameters on the friction drilling process, each time when the technology is introduced into production, it is necessary to select a mode for specific tasks, because even a slight change in the initial conditions can greatly affect the complex process behavior. In this regard, of particular interest is the use of new parameter selection methods, e.g., neural networks or machine learning algorithms applied in the works of Bustillo et al. [25] and Hynes et al. [39].

3 Hole geometry

The formation of bushings is the main reason for using friction drilling. Therefore, the drilling process optimization is mainly aimed at producing high-quality bushings to provide reliable threaded connections. When evaluating the bushing quality, it is first of all necessary to account for the type of connection and the direction of load application on the final product during operation.
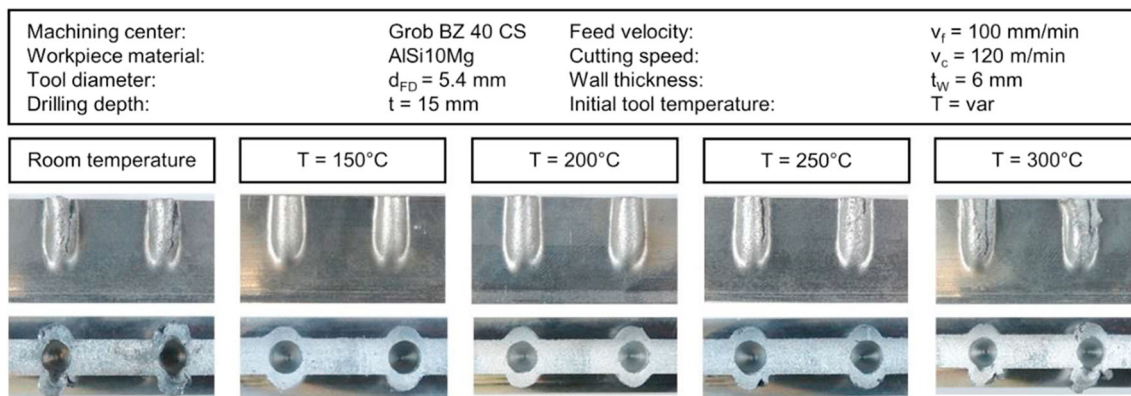
Machining center:	Grob BZ 40 CS	Feed velocity:	v_f = 100 mm/min
Workpiece material:	AlSi10Mg	Cutting speed:	v_c = 120 m/min
Tool diameter:	d_{FD} = 5.4 mm	Wall thickness:	t_W = 6 mm
Drilling depth:	t = 15 mm	Initial tool temperature:	T = var

| Room temperature | T = 150°C | T = 200°C | T = 250°C | T = 300°C |

Fig. 7 Quality of bores in the profile ends at different tool preheating temperatures [34]

In the general case, the thread strength can be determined by the formula [40]:

$$F_{sh} = \pi d L_{sc} K_g K_m \tau \qquad (1)$$

where d is the thread diameter, L_{sc} is the thread length, K_g is the thread fullness coefficient, K_m is the coefficient of inhomogeneous plastic strain distribution in thread turns over height, and τ is the shear strength of the material.

The practical use of this formula in the context of friction drilling is complicated for the following reasons. As already noted, a friction-drilled thread connection can be subjected to various operational loads: along the bolt axis, perpendicularly, or at a different angle. Another difficulty is the shear strength included in the equation. As will be discussed below, the material near the hole is hardened; therefore, the tabular value of the material strength cannot be used to calculate the connection strength. Also, recrystallization in the drilling process can cause the softening of the material.

From the viewpoint of increasing strength, it makes sense to increase the thread length, which is limited by the bushing height. The material removed from the hole during friction drilling flows both upwards and downwards, forming the upper and lower bushings, which can be determined by the formula:

$$\frac{\pi d^2}{4} \delta = V_{lb} + V_{ub} \qquad (2)$$

where V_{lb} and V_{ub} are the volume of the lower and upper bushings, respectively, δ is the workpiece thickness, and d is the hole diameter.

As established experimentally [41], the material density changes slightly during friction drilling, which allows us to neglect the loss of volume and equate both sides of the equation. The shape of the bushing can be simply represented as a truncated paraboloid for the purpose of calculating its thickness and height [42]. At first glance, this suggests that the bushing thickness and height depend only on the hole diameter and workpiece thickness. However, the volume ratio of the

upper and lower bushings varies depending on the axial force and spindle speed, up to a complete absence of the upper bushing (Fig. 8).

In practice, a threaded joint is most often produced by cutting the thread into the lower bushing, and the upper part is removed or expanded by a tool. This means that the excess material flowing upwards is used inefficiently and thus the usable length for thread making is reduced. Consequently, the technology optimization for a particular material involves the selection of such a spindle speed and axial force as to obtain a bushing of required length. From the viewpoint of bushing strength, its thickness, which decreases with height, should also be increased. As shown in drilling austenitic stainless steel pipes [43], the bushing thickness varies unevenly along the length depending on the technological mode. With increasing spindle speed, the bushing thickness decreases in the upper part and increases in the lower one. The thickness of the lower part also increases with increasing feed rate.

Major defects in friction drilling are cracking of the bushing and petal formation. These defects result from improper process parameters. According to Vergara et al. [44], the optimal parameters for high-quality bushing formation depend on the properties of the workpiece material. For example, for pure copper, it is preferable to perform drilling with high spindle speeds but low feed rate (1–2-mm thickness, 4.5-mm hole diameter, 4000 rpm, 50–100 mm/min). With the same workpiece thickness and tool diameter, α-brass should be drilled with low spindle speeds and medium feed rate (100–500 rpm, 100–300 mm/min), because this material is embrittled in high heating. Thus, it is not always possible to achieve a balance of the geometric characteristics of the hole and the absence of defects by optimizing the technological parameters.

For improving the quality of the formed bushing, Su et al. [45] proposed to use a counter-bore die for drilling with controlled material flow (Fig. 9). This approach was shown to eliminate the formation of cracks and petals. In addition, the formed bushing was more uniform in thickness.

In the work [46], threaded holes were produced by a combined method of dissimilar material joining on the following
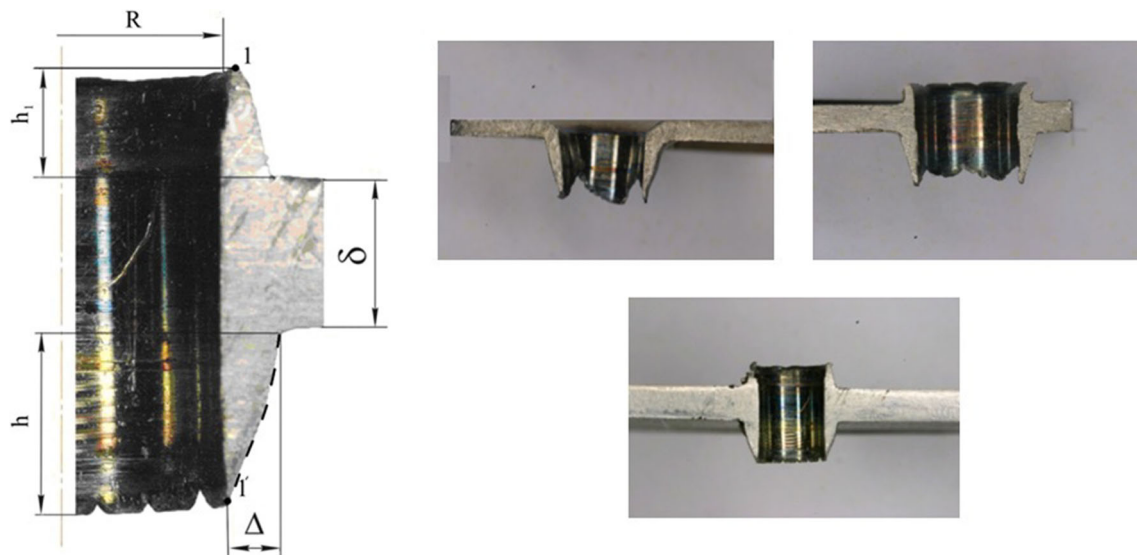
Fig. 8 Geometry of holes formed by friction drilling in sheet metal [42]

couples of materials: AISI 1045/Al 5754, AISI 304/Al 5754, and AISI 304/Al 6082. A drawback of this method is the formation of a gap between the joined sheets. The presence of the gap can lead to ingress of moisture and other contaminants between the sheets, their corrosion, and therefore shorter life of the joint. The gap can be reduced by varying the technological parameters. For example, it was unambiguously demonstrated that increasing the spindle speed reduces the gap size, as well as decreasing the tool feed rate. Nevertheless, within the spindle speed range of 1500–4500 rpm and the feed rate range of 150–450 mm/min, the smallest gap for the AISI 1045/Al 5754 couple was observed at a ratio of 3500 rpm to 150 mm/min. The gap formation was also shown by Lacalle et al. [47] when drilling AA5754 and S235 steel tube.

El-Bahloul [48] performed friction drilling of a cast aluminum alloy A380 workpiece sandwiched in between sheets of

316 steel, 6060 aluminum alloy, and red copper alloy. Optimization of technological parameters by fuzzy logic techniques confirmed that the smallest gaps between the surfaces and the largest bushing length are achieved at lower tool feed rates. The best quality holes were drilled in sandwiches with red copper.

4 Mechanical properties

One of the pioneering works of France [49] showed good applicability of friction drilling for joining tubular columns. Cantilever testing of a beam connected to a column revealed that an increase in the endplate thickness, column wall thickness, and a greater beam depth lead to an increase in stiffness and strength, which is characteristic not only of friction drilling.
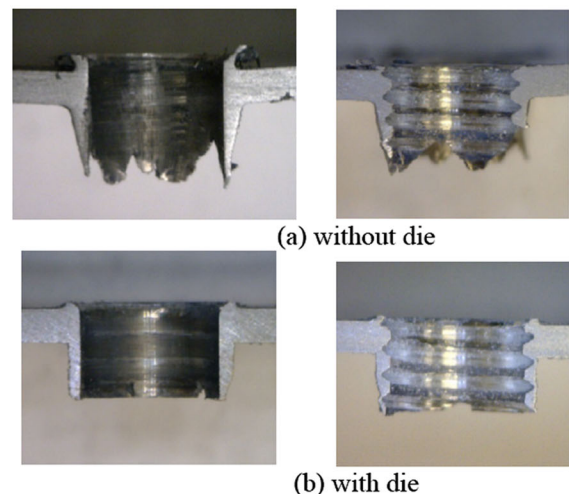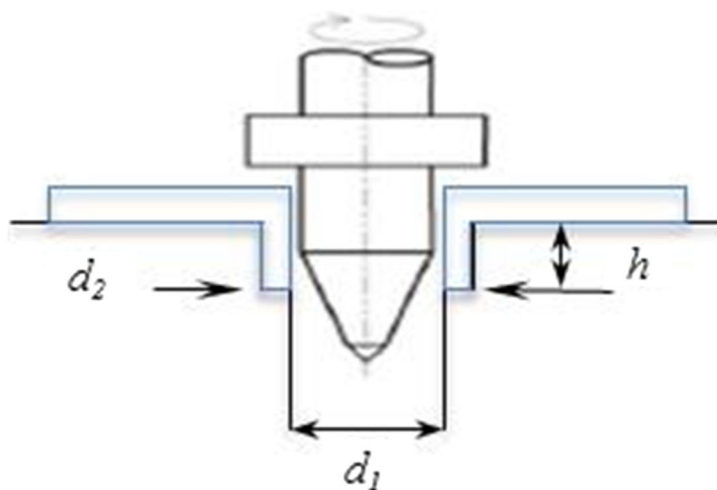

Fig. 9 Schematic of friction drilling using a counter-bore die and examples of bores drilled in aluminum alloy AA6061 with and without the die [45]

The microhardness of the material near the surface of contact with the tool is higher by 20–70% than in the initial material and decreases monotonically with increasing distance from the hole down to the value of the initial material. This was demonstrated for such materials as AISI 1020, 4130 steel, Al 5052 [50], brass [27], and AISI 304 [51] (Fig. 10).

In addition to the change in mechanical properties with distance from the hole, Kumar and Hynes [52] observed a change in microhardness along the bushing length on galvanized DP 600 steel. Deformation during friction drilling is complex, and the load varies non-linearly with time. As a result, each bushing region has its own thermal and deformation history, which affects its structure and properties. A total of 5 regions were distinguished: tail-end region, Luders band region, lower critical region, upper critical region, and bending region. The highest microhardness is achieved in the lower critical region, and the smallest one is observed in the upper critical region. It was also found that the bushing microhardness generally decreases with increasing heat release, i.e., increasing spindle speed. When drilling titanium alloy Ti-6Al-4V, microhardness, on the contrary, decreases by 25% near the friction surface [35]. And the longer the thermal effect, the greater the microhardness decrease, associated with the structural transformations of the material.

Another important factor of strength, along with the material properties and drilling mode, is the thread cutting method. Wittke et al. [53] studied the mechanical characteristics of internal threads produced by friction drilling in flat profile specimens of 6061 aluminum alloy. Comparisons were made between different manufacturing techniques, such as thread tapping (or cutting), forming, and milling. As an object of comparison, the authors used a thread drilled in a bulk material specimen by a conventional method. The tapped thread showed the best results in both cases, because tapping causes surface layer hardening. Due to the elongated shape of the bore, the friction-drilled thread withstood half the load and

30% lower amplitude in fatigue testing. Similar results for AlSi10Mg and AZ31 alloys were observed in a different paper [54]. The oval shape of the hole in AlSi10Mg alloy led to lower joint strength compared to AZ31 (Fig. 11). It is worth noting, however, that the hole diameter changes after thread tapping. As reported in the paper [55]: "Tap manufacturers usually recommend initial diameter lower than the just geometrical one."

Later, the same authors [56] studied the mechanical properties of an internal thread produced by friction drilling in a flat AZ31 magnesium alloy profile. As in the work [34], drilling was carried out with tool preheating to 200°C. In general, preheating had a favorable effect. As shown by the results of X-ray computed tomography, preheating contributed to a higher quality of the formed thread in the hole. Obviously, this is main reason for the high strength of the threaded joint drilled with preheating, since preheating did not affect the thread microhardness and fatigue characteristics. Drops in the load curves are explained by thread stripping. With increasing test temperature, the thread failure was softer, which led to higher strength and ductility values.

Different authors understand the quality of the hole differently, depending on the focus of the investigation. In general, the hole quality is an integral characteristic that includes geometric characteristics, structure of the material at different hierarchical levels, and defects. The strength of the friction-drilled joint generally depends on the bushing geometry, thread cutting method, and strength properties of the material. As shown in Section 2, the joint strength is proportional to the length and thickness of the bushing. It can be reduced by the presence of defects in the form of petals, cracks, burrs, and others. The strength properties of the bushing material directly depend on the state of the initial material as well as on the temperature and deformation conditions during drilling. The effect of technological parameters on the geometric and strength characteristics of the bushing can be contradictory.
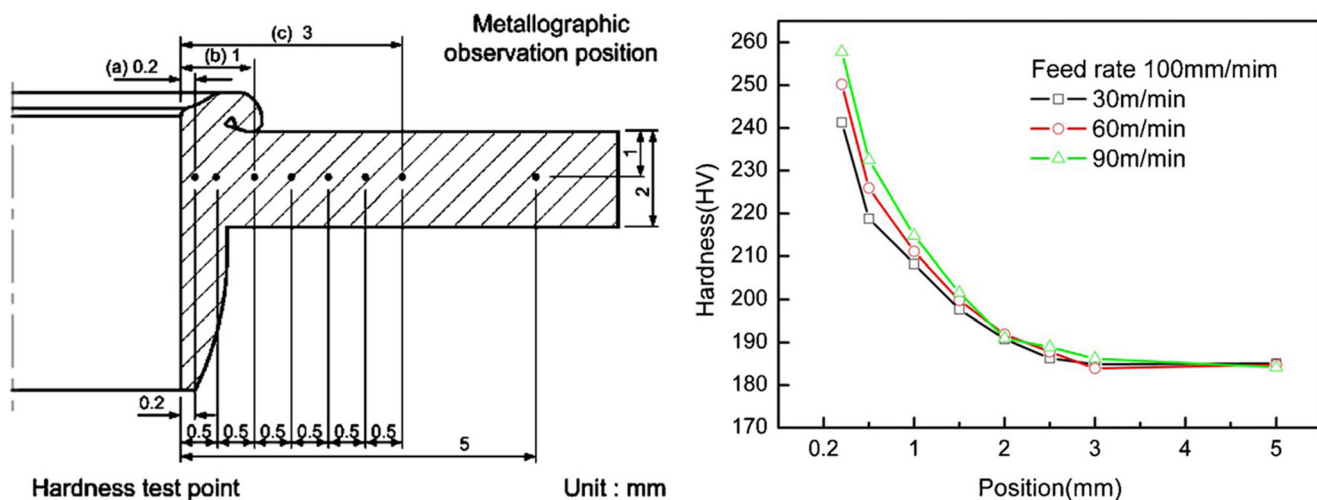

Fig. 10 Hardness test points and hardness at different distances from the hole edge for different drilling speeds in AISI 304 [51]
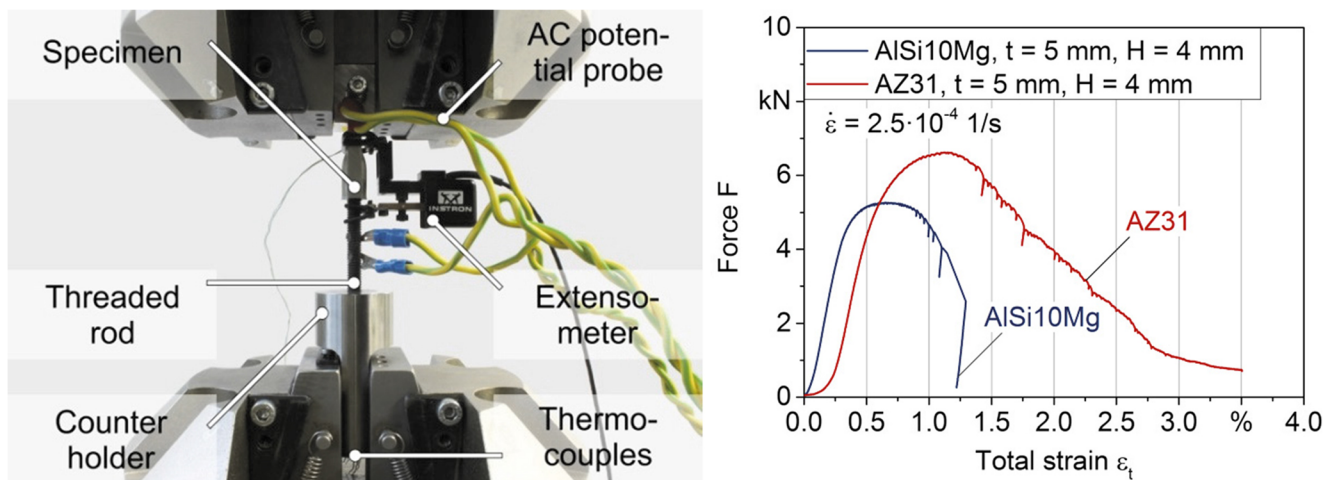
Fig. 11 Experimental setup for mechanical testing of a friction-drilled thread in a flat profile, and force vs. total strain curves [54]

For example, according to Engbert et al. [57] who studied friction drilling of an extruded AlMgSi0.5 alloy profile reinforced with X10CrNi18-8 steel wire, an increase in the spindle speed (and hence temperature) led to a better bushing geometry and material softening, but the thread strength generally decreased. The presence of the reinforcing steel wire, which retains heat in the material after drilling, did not significantly affect the thread strength. This case shows that the friction drilling process involves multiple factors. In particular, the presence of visual bushing defects may not always indicate a low strength of the thread. One of the most important quality parameters is the structure of the material around the hole.

5 Microstructure

The extruded material of the bushing is subjected to severe deformation and elevated temperatures during friction drilling, due to which its microstructure is refined [50]. This is true for steels, aluminum alloys, and commercially pure titanium. In addition, elevated temperatures and deformation affect the material around the hole. The influence can extend to a distance of 5–7 mm, and several structural zones can be distinguished in the material (Fig. 12). As shown in the works of Eliseev et al. [58–60] on aluminum alloys, the mechanisms and effects of friction drilling are similar to those of friction stir welding, and therefore the structural zones can be denoted in the same way. Stir zone (SZ), which is in direct contact with the tool and is subjected to severe plastic deformation and elevated temperature; thermomechanically affected zone (TMAZ), which is not in contact with the tool but is affected by deformation and elevated temperature; and heat affected zone (HAZ), which is only affected by heat.

The SZ contains recrystallized equiaxed grains of solid solution. During friction drilling of AA2024 sheet metal, the initial elongated grains with sizes 69×21 μm were reduced to

3 μm. Grains in the TMAZ grew more than 2 times, became even more elongated, and turned upwards and downwards in the deformation direction. The TMAZ also has localized deformation regions. The material layers move relative to each other and are partially recrystallized. This explains differences in microhardness values in the given zone. The grain structure of the HAZ cannot be characterized because this zone is etched in aluminum alloys.

Severe plastic deformation also causes the dissolution of intermetallic compounds in the material around the hole. Scanning electron microscopy with phase contrast (Fig. 13) demonstrates a sharp contrast of the structure at the interface between the SZ and TMAZ. Bright objects in the image are incoherent second phase particles. The volume fraction of these particles in the SZ decreases twice and their average size is reduced 3–5 times compared with the original aluminum alloys AA2024, AA3005, and AA5056. Since the friction drilling time is short, the dissolved particles do not have time to precipitate again in the same amount, as occurs during friction stir welding. In the TMAZ, the volume fraction and average size of incoherent second phase particles can both decrease and increase, depending on the deformation conditions and the amount of heat. The distribution of particles also varies depending on their location in the layer of locally deformed material.

The described feature is also characteristic of the SZ. As shown for AA2024 alloy [61], the size and volume fraction of semi-coherent second phase particles change with distance from the hole. In particular, the particle size at a distance of 350 μm was smaller than at a distance of 90 μm from the hole (Fig. 14). The volume fraction of particles remained almost unchanged. In this case, the decisive factor for the mechanical properties is the dispersion factor D, which is the ratio of volume fraction F_v to particle size d. The higher the dispersion factor, the higher the microhardness value and material strength σ:

Fig. 12 Structural zones of the hole cross-section in AA2024 (a); grain structure in the stir zone (b) [58]
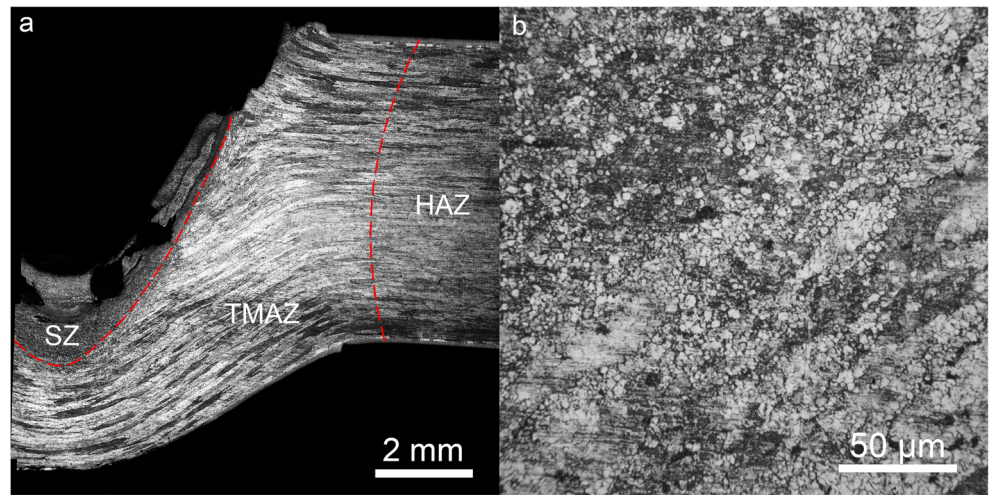
$$D = \frac{F_v}{d} \propto \sigma \qquad (3)$$

Since the temperature is insufficient for dissolution, the particles during friction drilling dissolve due to deformation. The greatest refinement of semi-coherent particles was observed at a distance of 350 μm from the hole. Such a particle distribution illustrates the discrete nature of material deformation around the tool in friction drilling according to the concept of adhesive/cohesive layer-by-layer material transfer.

Hynes et al. [39] showed that Luders bands may appear on the inner surface of the bushing in galvanized steel under the influence of elevated temperatures (798°C) and axial force, and the band spacing is uneven due to inhomogeneous deformation in friction drilling. In general, the microstructure of the material around the hole is poorly studied. However, it is already known that the material has a complex heterogeneous structure. The detected structural features are similar to FSW joints.

6 Numerical modeling

In the work [19], heat transfer during friction drilling is described by the equation

$$\rho c \frac{\partial T}{\partial t} = k \left[\frac{\partial^2 T}{\partial x^2} + \frac{\partial^2 T}{\partial y^2} + \frac{\partial^2 T}{\partial z^2} \right] + G \qquad (4)$$

where T, ρ, and t are respectively the temperature, material density, and time; k and c are the specific thermal conductivity and heat capacity; and G is the heat release rate density determined by the sum of the heat fluxes due to friction $\dot{q}_f$ and plastic deformation $\dot{q}_p$:

$$G = \dot{q}_f + \dot{q}_p \qquad (5)$$

$$\dot{q}_f = 2\pi R N \mu F_n \qquad (6)$$

$$\dot{q}_p = \eta \sigma \dot{\varepsilon}^{pl} \qquad (7)$$

where R is the tool radius, N is the spindle speed, μ is the coefficient of friction, F_n is the normal force, η is the inelastic

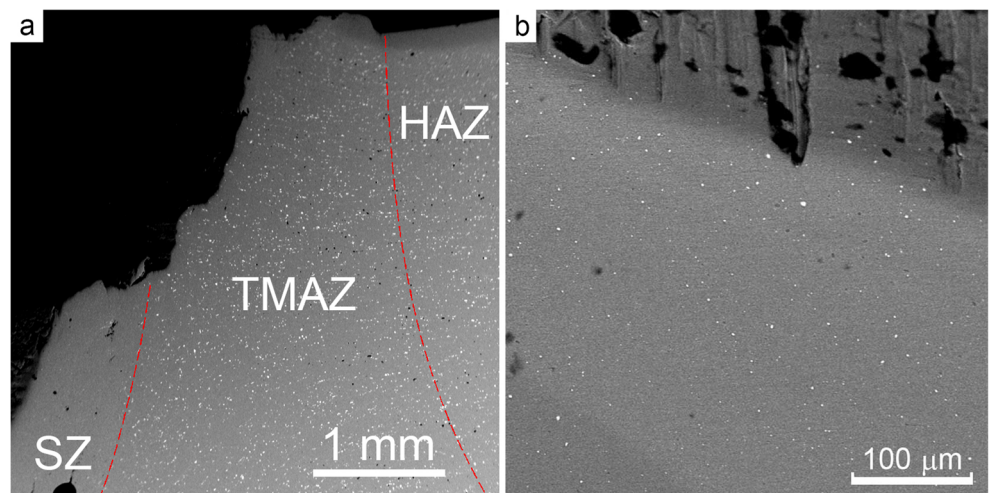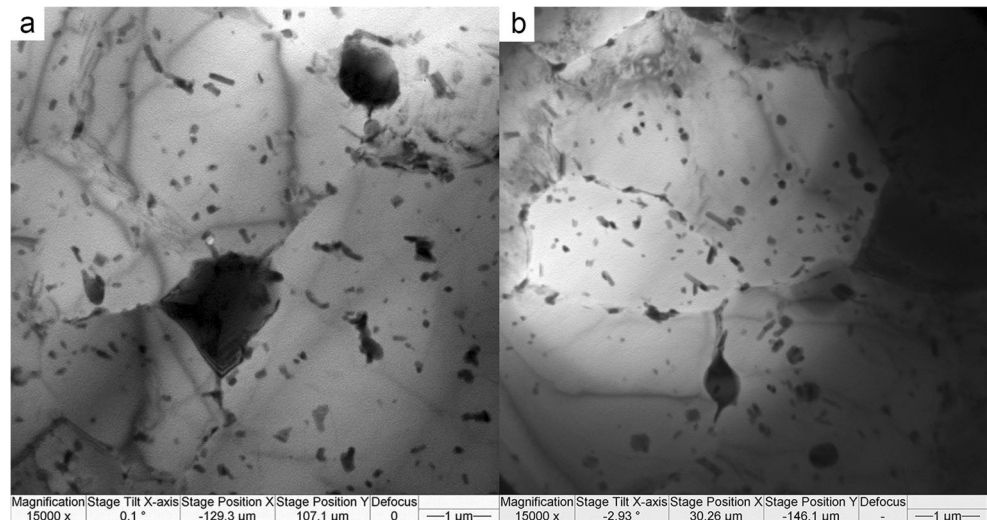**Fig. 13** BSE image of a friction-drilled hole in AA2024 (a) and AA5056 (b) [58, 60]

Fig. 14 Bright field TEM image of AA2024 microstructure in the SZ at 90 μm (a) and 350 μm (b) below the friction-drilled hole surface [61]

Magnification	Stage Tilt X-axis	Stage Position X	Stage Position Y	Defocus
15000 x	0,1 °	-129,3 µm	107,1 µm	0

Magnification	Stage Tilt X-axis	Stage Position X	Stage Position Y	Defocus
15000 x	-2,93 °	30,26 µm	-146,1 µm	-

part of heat, σ is the true stress, and $\dot{\varepsilon}^{pl}$ is the plastic strain rate.

A different method for heat transfer determination was proposed by Bilgin et al. [62]. Based on the technological parameters, the torque power P_c and the axial power P_f are calculated, the sum of which is reduced to the heat energy:

$$Q = P_c + P_f \tag{8}$$

$$P_c = M\omega = M2\pi N \tag{9}$$

$$P_f = F_n V \tag{10}$$

where M is the torque, ω is the angular velocity, and V is the feed rate.

In fact, these methods look at the solution of the problem from different sides. In the case of Eqs. (6)–(7), specific physical processes that occur with the material — friction and deformation — are considered. On the one hand, this is the correct approach; however, the problem is in the physical properties of the material itself. The material during severe plastic deformation is in a unique state, so there is no way to reliably establish its stress, friction coefficient between surfaces and other its properties. In fact, the strain rate cannot be determined experimentally. Therefore, any estimates by this method can only be verified indirectly. On the other hand, Eqs. (9)–(10) are very easy to apply, all quantities are experimentally determined, and the actual total energy input to the system can always be calculated. And herein consists the disadvantage of the method — it is impossible to simulate without experiment. In addition, both methods do not take adhesion into account. An important mechanism of the friction drilling (like friction stir welding) is adhesive transfer. During drilling, the surface of the tool grips the material, transfers it to another location, slips, adhesion occurs, and a new transfer occurs. That is, sliding friction and mass transfer occur alternately. Both of these processes consume energy, but so far it has not been possible to determine the relationship between them. Nevertheless, attempts to describe the process continue.

Miller [19] also performed analytical modeling of torque M and thrust force F during drilling separately for each tool part. The thrust force and torque for the conical part are

$$F = \pi p \left(h_2^2 - h_1^2 \right) \tan^2 \frac{\theta}{2} + \mu_a p \pi \left(h_2^2 - h_1^2 \right) \tan \frac{\theta}{2} \tag{11}$$

$$M = \frac{2\pi\mu p \left(h_2^3 - h_1^3 \right) \tan^2 \dfrac{\theta}{2}}{3\cos \dfrac{\theta}{2}} \tag{12}$$

where p is the pressure; h_2 and h_1 are respectively the distances from the cone apex to the upper and lower surfaces, the difference of which determines the truncated cone height; θ is the cone apex angle; and μ_a is the coefficient of friction in the axial direction.

In the cylindrical part:

$$F = 2\pi\mu_a pRh_3 \tag{13}$$

$$M = 2\pi\mu p R^2 h_3 \tag{14}$$

where h_3 is the height of the cylindrical part.

This model is in good agreement with the experimentally measured thrust force in friction drilling. Later, the model data for calculating the thrust force [63] and torque [64] were improved for the conical part as follows:

$$F = \pi p \left(h_2^2 - h_1^2 \right) \tan^2 \frac{\theta}{2} + 2\pi\mu p \frac{v}{\omega} (h_2 - h_1) \cos \frac{\theta}{2} \tag{15}$$

$$M = \pi\mu p \frac{2\tan \dfrac{\theta}{2}}{\cos \dfrac{\theta}{2}} \left(h_2^3 - h_1^3 \right) - \pi\mu p \frac{v^2}{\omega^2} (h_2 - h_1) \cos \frac{\theta}{2} \tag{16}$$

where ω is the angular velocity, and v is the feed rate.

Meanwhile, the article [63] aims primarily to calculate the friction coefficient, which is derived from Eq. (15) when the force is experimentally determined.

For the cylindrical part, the thrust force and torque were transformed as follows [64]:

$$F = \frac{2\pi\mu p R h_3 v}{\sqrt{v^2 + \omega^2 R^2}} \qquad (17)$$

$$M = \frac{2\pi\mu p R^3 h_3 \omega}{\sqrt{v^2 \omega^2 R^2}} \qquad (18)$$

The thrust force calculated by this model is somewhat closer to the experimental results. Thus, the model in [19] is not relevant at this time and is given as a historical reference.

A similar modeling performed by Raju and Swamy [65] showed that an increase in the spindle speed and feed rate increases the true strain in friction drilling, but a too large spindle speed increase leads to the formation of an irregular bushing, due to which the true strain is sharply reduced.

Dehghan et al. [66] carried out numerical modeling of the friction drilling of an aluminum alloy by a three-dimensional finite element method. They used the Johnson–Cook model that depends on temperature and strain rate. Thus, the yield stress:

$$\overline{\sigma}_y = \left(A + B\left(\overline{\varepsilon_{pl}}\right)^n\right)\left[1 + C\ln\frac{\dot{\overline{\varepsilon_{pl}}}}{\dot{\varepsilon}_0}\right]\left(1 - \left(\frac{T - T_{tran}}{T_{melt} - T_{tran}}\right)^m\right) \qquad (19)$$

where A, B, C, and n are respectively the initial yield stress, hardening modulus, strain rate sensitivity, and strain hardening exponent; m is the thermal softening effect; $\overline{\varepsilon_{pl}}$, $\dot{\overline{\varepsilon_{pl}}}$, and $\dot{\varepsilon}_0$ are the equivalent plastic strain, equivalent plastic strain rate, and reference strain rate; T is the current temperature; and T_{melt} and T_{tran} are the melting and transition temperatures.

Since the tool penetrating the workpiece breaks the material, a failure criterion is needed that would not reach 1:

$$D = \int \frac{1}{\varepsilon_f} d\overline{\varepsilon_{pl}} \qquad (20)$$

The fracture strain was defined as:

$$\varepsilon_f = \left(d_1 + d_2 e^{-d_3\frac{p}{\sigma}}\right)\left[1 + d_4\ln\frac{\dot{\overline{\varepsilon_{pl}}}}{\dot{\varepsilon}_0}\right](1 + d_5\theta) \qquad (21)$$

where d_1, d_2, d_3, d_4, and d_5 are experimentally determined constants, and p is the hydrostatic pressure.

Modeling showed that the highest stresses are achieved in the contact area at the initial stage of drilling. In this case, the inverse dependence of temperature and stress points to material plasticization without reaching the melting temperature. The shape of the hole is basically similar to the real one, but there are some flaws. In particular, the wall thickness and bushing height are lowered. The inner surface of the hole is irregular, which does not correspond to the experiment (Fig. 15). In addition, the weaknesses of the model include an abundance of constants, whose physical sense is unclear. In the more recent works of these authors, it has not yet been achieved to bring the shape of the hole model closer to that of a real hole [67].

Kumar and Hynes [68] modeled the friction drilling of galvanized steel by the finite element method using DEFORM-3D software. The equations of continuity, conservation of momentum, and conservation of energy were solved simultaneously during modeling. The mechanical properties were determined as follows:

$$\delta_t = 2\dot{\varepsilon}\mu \qquad (22)$$

where $\dot{\varepsilon}$ is the strain rate, δ_t is the deviatoric stress tensor, and μ is the viscosity.

The energy conservation equation corresponds to the above given Eq. (4), but the heat release rate is described differently. Only the component that is caused by plastic deformation is taken into account and is described by Eq. (7). The modeling results for material deformation during friction drilling showed good agreement with the experiment. The calculated bushing length was 5.98 mm, and that measured on the experimental sample drilled with the same parameters was 5.94 mm. However, the use of this approach in itself is highly disputable. Despite the high temperature, the material is still a solid. Some problems occur in viscosity determination during severe plastic deformation at high strain rates. In particular, the problem is the experimental verification of viscosity.

Modeling also revealed a non-uniform temperature distribution along the bushing length. The maximum temperatures are reached close to the middle plane of the hole and amount to 709°C. The temperature measured experimentally by thermal imaging was 747°C, which is close to the calculated value. The inhomogeneity of the temperature distribution was confirmed by a microstructural study. It was found that the maximum temperature region in the material around the hole contains larger grains.

In fact, such a result was fairly obvious from the experimental results. In this context, so far, simulation of frictional drilling can hardly provide any new scientific knowledge or improve the understanding of physical processes. At least, within the framework of the described approaches. First, these approaches do not take into account the adhesive nature of drilling. Second, the modeling methods themselves were not originally designed to simulate severe plastic deformation. In particular, for example, element birth and death techniques lead to distortions at high strains and strain rates. Agreement with experimental data is often achieved by using empirical coefficients with unclear physical sense. Nevertheless, work is

Fig. 15 Comparison of cross-sectional view between experimental and simulated drilled hole [66]
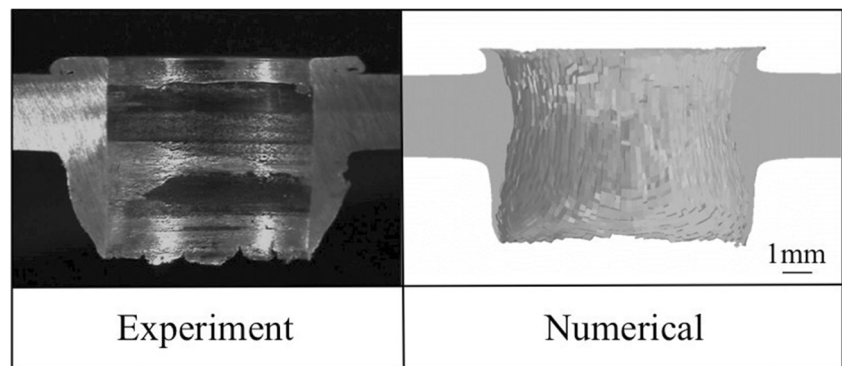
continuing. An adequate prediction of the hole geometry will be a success in this field. This can be used to solve technical problems, such as the selection of technological parameters.

7 Flow drill screwdriving

Flow drill screwdriving is a technological process that combines hole making with bushing by friction drilling, thread forming, and immediate joining of parts. In so doing, a screw is used as both the fastener and the tool. The earliest patent for this method was issued to Amanda Kay Freis in 2013 [69] and is described as a technique for fastening two or more sheets with and without gaps.

The process steps of flow drill screwdriving are in general similar to those of friction drilling (Fig. 16): (1) the workpiece is heated by friction from the rotating fastener (2000–6000 rpm); (2) the rotating fastener penetrates the workpiece material; (3) an extrusion or bushing is formed while the fastener continues to penetrate; (4) the rotating fastener forms a thread in the bushing material (~ 2000 rpm); (5) the screw is driven into the hole (~ 200 rpm); and (6) the screw is tightened to the appropriate value. The highest axial force is achieved in step 3 of bushing formation, and then decreases in threading, screwing, and tightening. The load is one of the most important parameters in flow drill screwdriving from the viewpoint of obtaining the correct joint geometry. According to [70], the

higher the fastener load, the higher the deflection of the joined sheets.

As in friction drilling of sandwiches, a gap is formed between the upper and lower sheets in flow drill screwdriving. The gap size is determined by the ratio of technological parameters. This gap is dangerous in terms of contaminant accumulation and corrosion in the joint material. As shown by Scholz et al. [72] in corrosion tests on lap-shear specimens of dissimilar materials AlMgSi1–X5CrNi18-10, AlMg4.5Mn–X5CrNi18-10, AlMg4.5Mn–HC340LA, AZ31–AlMg4.5Mn, the tensile strength does not decrease significantly due to corrosion, but the fatigue life of the joints is reduced. The gap itself also reduces the joint strength. For example, the gap in coach peel specimens of AA6082 reduces by 7% the joint strength [73]. Typical defects for flow drill screwdriving are chip formation, bushing fracture, and sheet deflection. Chips are formed in high-speed drilling; bushing fracture and deflection occur at a low spindle speed but high load [74]. These defects deteriorate the machinability conditions, but have almost no effect on the axial strength of the joint, as was observed in joining HCT780X steel and AA5152-O.

Meschut et al. [75] compared the strength of lap joints obtained by conventional and new methods: clinching, self-pierce riveting (SPR), flow drill screwdriving (high-speed bolt joining RIVTAC), self-pierce riveting with solid rivets (SSPR), resistance element welding (REW), friction element welding (FEW), and resistance spot welding (RSW). As can
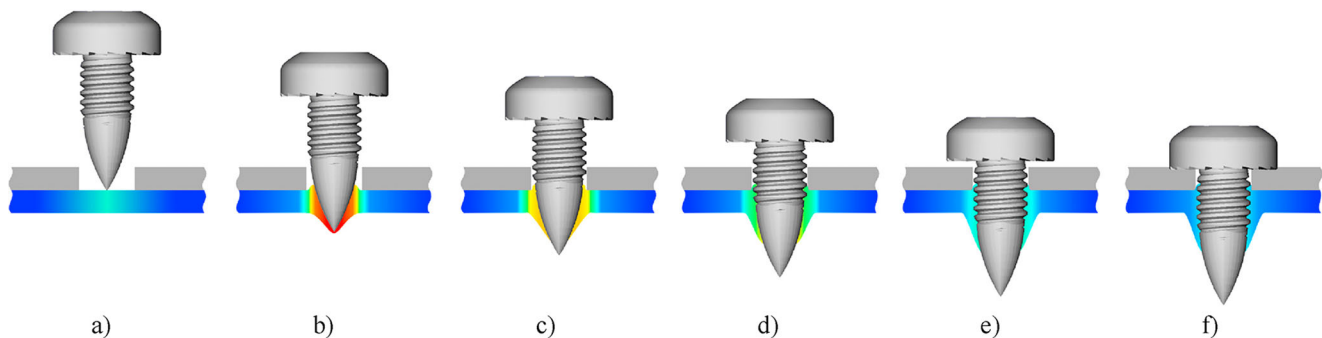

a)   b)   c)   d)   e)   f)

Fig. 16 Stages of the flow drill screwriving: (**a**) warming up, (**b**) material penetration, (**c**) bushing forming, (**d**) thread forming, (**e**) full thread engagement, (**f**) tightening [71]

be seen from the diagrams in Fig. 17, the flow drill screw joint (RIVTAC curve) is second only to the FEW joint in terms of strength.

The estimation of heat release rate in flow drill screwdriving, proposed by Skovron et al. [76], resembles Eq. (6) in Section 6, but normal force is calculated using yield strength σ_y and contact area A:

$$F_n = \sigma_y A \tag{23}$$

The additional heating of the AA6053-T5A workpiece to 247°C [76] did not lead to a change in the joint geometry and a decrease in the gap size, but reduced the process time by almost half. After heating to 143°C, the microhardness of the material near the fastener decreased, but the overall joint strength increased due to better contact between the fastener and the hole. Heating to high temperatures weakens the joint. Composite structures of reinforced plastics and metals have recently gained great popularity, especially in automotive industry. The use of such materials reduces the weight of products and, consequently, air pollution. Great differences in the properties of metals and plastics determine a very limited number of methods for their joining. The most commonly used one is riveting. Flow drill screwdriving can also be used for joining plastics and metals.

The main problem in metal/plastic joining is the formation of plastic chips, which complicates thread forming, reduces the thread quality and the overall joint strength. This problem can be solved by selecting a tool that would cut off the top layer of plastic material and remove chips from the joint zone, with a suitable configuration for metal sheet drilling. As shown by Nagel and Meschut [77] for joints of fiber-reinforced plastic with thermoplastic or thermosetting matrix and HC340LAD steel or EN AW-6181 aluminum sheets, the largest push-out strength is observed for screws with a cutting tip with a hole.

Szlosarek et al. [78] conducted mechanical tests with different loading angles on a sandwich of carbon fiber-reinforced plastic and EN-AW6060-T6 aluminum alloy joined by flow drill screwdriving. The test results showed that the loading angle does not affect the maximum joint strength, but strongly affects its ductility. The larger the angle, the lower the ductility. In similar tests performed by Sonstabo et al. [71] on AA6061-T6 aluminum alloy joints, the highest strength was observed in shear, i.e., at a loading angle of 0° (Fig. 18). In tensile tests and combined tensile-shear tests, the joint failure occurred by thread stripping in the bottom sheet material. Shear tests resulted in failure of the bottom sheet. The general failure modes observed in tests on single connectors and components were screw rotation, screw pull-out, screw push-out, and screw fracture. The anisotropy of the mechanical properties of sheet metal had no effect on the mechanical test results. Thus, flow drill screwdriving showed good applicability in components under complex loading conditions.

In their subsequent paper [79], the authors carried out mechanical tests on a component made of aluminum alloys AA6005T5 and AA6060T6 connected by flow drill screwdriving. The results showed similar deformation behavior of the component under dynamic and quasi-static loading (Fig. 19).

The failure of 6082 aluminum alloy lap-shear specimens under quasi-static and cyclic shear loading occurs in different ways [80]. The most frequent situation under quasi-static loading is the failure of the upper sheet to screw fracture. Under cyclic loading, failure is most often observed in the lower sheet. The measurements of residual stresses in AA6063-T5A sheets joined by flow drill screwdriving [81] revealed the presence of high tensile stresses, which decreased with increasing distance from the fastener. This behavior was

Fig. 17 Comparative strength of lap joints produced by different techniques [75]
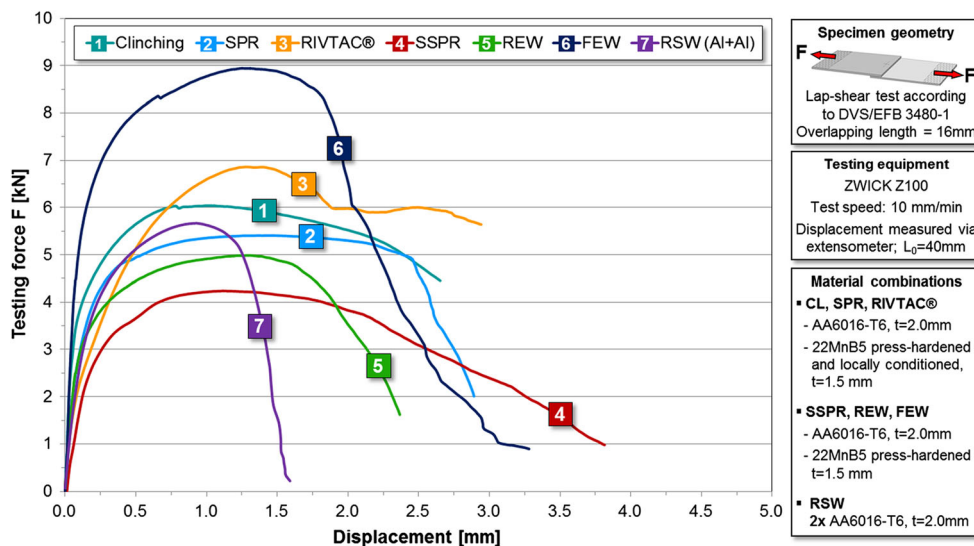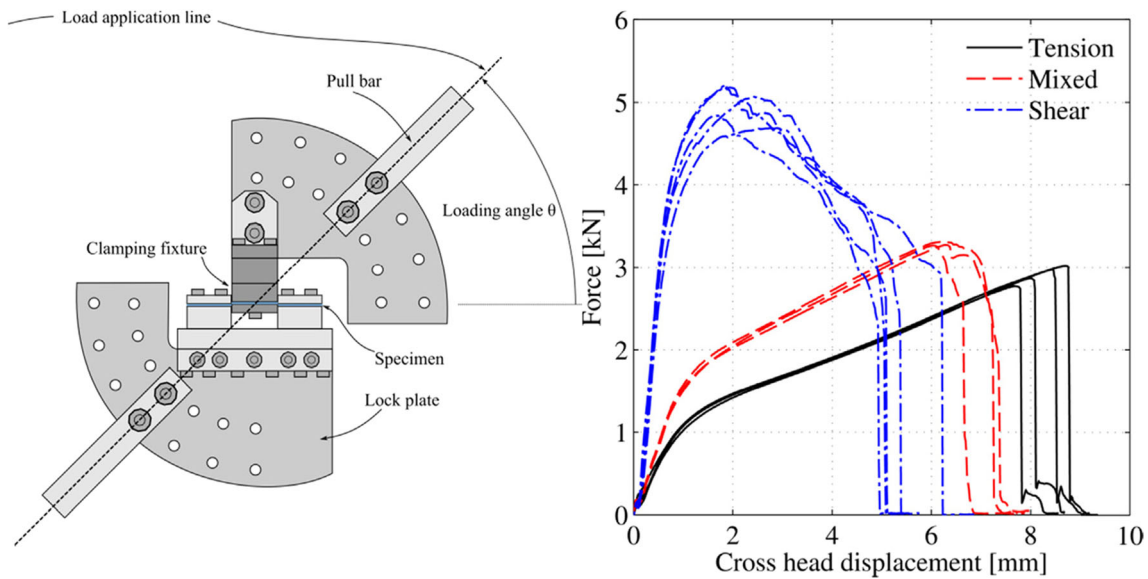
Fig. 18 Schematic illustration of the testing rig and force vs. displacement curves from cross tests [71]

observed in all directions. With increasing load during drilling, the residual stresses increased in the upper sheet but reduced in the lower one.

Modeling of the mechanical properties of flow drill screw connections by existing methods generally yields values close to experimental ones [82–84]. Nevertheless, for both assemblies and single connections, model calibration is still required. The problem here lies, in our opinion, in the use of material constants. In fact, the microstructure of the material around the hole has a complex gradient. This also results in a gradient of properties, which has been shown in the previous sections. Actually, very little is known about the properties of this new material around the hole. The microstructure of such joints has not yet been studied at all due to the novelty of the technique, which nevertheless has proved to be efficient for specific applications. Also one of the serious problems of the technology is the failure of the fastener. Since the tool is also a

fastener, it is not economical to produce it using expensive materials such as tungsten carbide. Fasteners are often made from case hardened mild steel. However, such material is not suitable even for single drilling of high-strength alloys. Therefore, application of the technology has so far been limited to relatively soft materials.

8 Summary

Despite the long history of friction drilling, this technology is still new, relevant, and developing. It has been the subject of extensive research over the past decade and is actively introduced into production as one of the most technologically advanced, environmentally friendly, and economical way to produce thread connections of thin sheet materials. The obvious ways to improve friction drilling are the selection of new tool
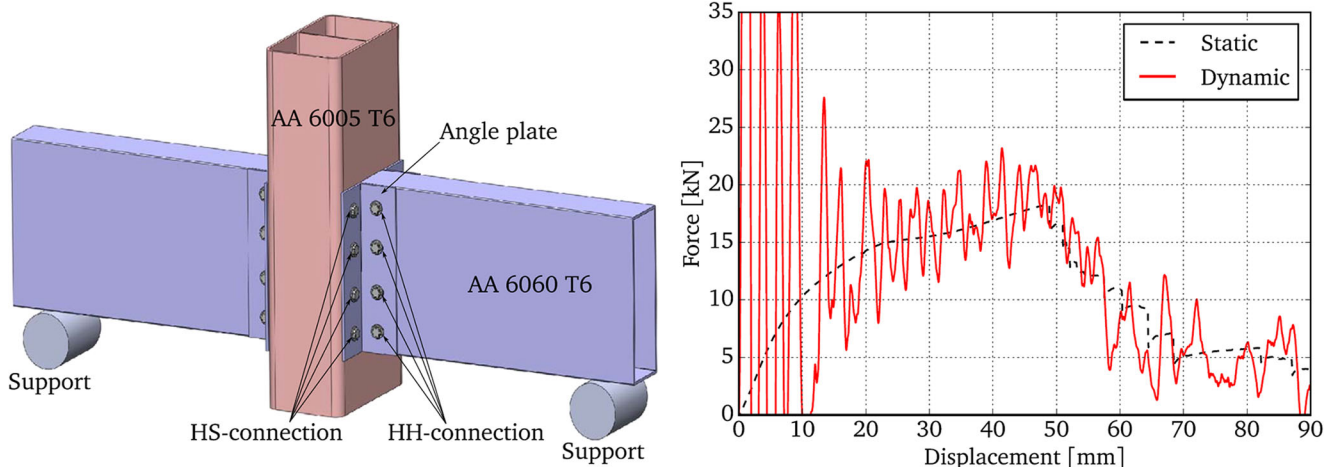

Fig. 19 Model of the test specimen and force vs. displacement curve of dynamic test compared to quasi-static test [79]

configurations and coatings (especially for titanium alloy drilling); optimization of technological parameters, including using variational analysis and neural networks; and the use of supporting means, such as additional heating/cooling sources and special dies. A breakthrough friction drilling technology of a new generation is flow drill screwdriving. It combines the well-known steps of making a threaded connection, but at an advanced technological level.

Today, friction drilling and its modification are successfully applied to produce high-quality threaded joints in most homogeneous non-ferrous and steel structural sheet materials. The effect of technological parameters on heat generation and deformation during friction drilling, which determine the joint quality, is well studied. Quality is generally understood as an integral characteristic of various properties of the material around the hole: bushing geometry, structural state that determines the material strength, the absence of defects, and hole surface roughness. Most of the literature investigates the influence of technological parameters on the joint strength, on its relationship with geometry, microhardness, and existing defects. Threads are most often formed in the lower part of the bushing, so the drilling modes are selected in such a way as to increase its length and to make it uniform along the length. These aims are usually achieved with high spindle speeds. Dangerous effects in the high-speed mode are the overheating, structural changes, and softening of the drilled material, which is typical, e.g., of thermally hardened aluminum alloys or α-brass. However, there are very few microstructural studies of the bushing material due to the complexity of research. The microscopic dynamics of the drilling process is not understood, although the mechanics of drilling and heat generation are well studied in view of the presence of adequate models. However, of course, it will take a long time to be able to solve the technical problems of selecting drilling parameters within the framework of existing models. The problem here is that the material around the hole is poorly understood. Another problem is the inadaptability of existing approaches for modeling such complex processes of severe plastic deformation. It has also been established that friction drilling is similar to friction stir welding. The material around the hole undergoes severe plastic deformation at elevated temperatures (up to 0.85 T_m) and is extruded into a bushing, with some structural changes. The resulting structural zones can be called in the same way: stir zone, thermomechanically affected zone, and heat-affected zone.

In view of the current technological trends, more and more researches are oriented towards the connection of dissimilar materials, titanium alloys, metal, and polymer composites, which is a specific subject. It poses new requirements for tool durability (especially for titanium alloys), process details (e.g., removal of polymer chips), and joint quality control. Consequently, further researches will be aimed at improving technology for new advanced materials and developing the physical foundations of friction drilling.

Declarations

Ethical approval Not applicable

Consent to participate Not applicable

Consent to publish Not applicable

Competing interests The authors declare no competing interests.

References

1. Streppel AH, Kals HJJ (1983) Flowdrilling: a preliminary analysis of a new bush-making operation. Annals CIRP 32(1):167–171

2. Boopathi M, Shankar S, Kanish T (2017) Investigation of surface texture generated by friction drilling on Al2024-T6. Mech Mater Sci Eng 9. https://doi.org/10.2412/mmse.1.19.706

3. Pereira O, Urbikain G, Rodrigues A, Calleja A, Ayesta I, Lopez de Lacalle LN (2019) Process performance and life cycle assessment of friction drilling on dual-phase steel. J Cleaner Prod 213:1147–1156

4. Sobotova L, Kralikova R, Badida M (2015) The analysis of chosen material properties at thermal drilling. Key Eng Mater 635:35–40

5. Dekkers GJ (1993) Flowdrill technical guide. Flowdrill, Holland

6. Enghauser WL (1929) Method of forming manifolds, US patent #1906953.

7. Leroy A (1957) Procédé et outil de formation de collets, et collets résultant de ce proceed, French patent #1189384.

8. Van Geffen JA (1974) Piercing tools, US patent #3939683.

9. Hoogenboom AJ (1982) Flow drill for the provision of holes in sheet material, US patent #4454741.

10. Dekkers GJ (1984) Flowdrill, particularly adapted to be used in a hand drilling machine, European patent #0150518 A1.

11. Head GD Jr, Le Master WC, Bredesky LP Jr, Winter DC (1982) Flow drilling process and tool therefor, US patent #4428214.

12. El-Bahloul SA, El-Shourbagy HE, Al-Makky MY, El-Midany TT (2013) Thermal friction drilling: (a review). 15th International Conference on Aerospace Sciences & Aviation Technology, ASAT – 15.

13. Alphonse M, Raja VKB, Logesh K, Nachippan MN (2017) Evolution and recent trends in friction drilling technique and the application of thermography. IOP Conf. Series: Mater Sci Eng 197: 012058

14. Gajjarkar B, Kamble N, Kamble Y (2017) A comprehensive review on influence of process parameters by a novel method form drilling technique. J Emerg Technol Innovative Res 4(6):16–20

15. Kerkhofs M, Van Stappen M, D'Olieslaeger M, Quaeyhaegens C, Stals LM (1994) The performance of (Ti,Al)N-coated flowdrills. Surf Coat Technol 68(69):741–746

16. Prabhu T, Arulmurugu A (2014) Experimental and analysis of friction drilling on aluminium and copper. Int J Mech Eng Technol 5(5):130–139

17. Alphonse M, Bupesh Raja VK, Rama Chandra LV, Venkata Subbaiah B, Sai Uday Kiran R, Gopala Krishna V (2021) Experimental investigation and optimization of surface treated and coated friction drilling tool for AZ31B magnesium alloy. Mater Today Proc 44(5):3760–3766

18. Mutalib MZA, Ismail MIS, Jalil NAA, As'arry A (2018) Characterization of tool wear in friction drilling. Jurnal Tribologi 17:93–103

19. Miller SF (2006) Experimental analysis and numerical modeling of the friction drilling process. Ph.D. Thesis, University of Michigan, Ann Arbor, MI, USA, 2006.

20. Ku W, Chow H, Lin Y, Wang D, Yang L (2011) Optimization of thermal friction drilling using grey relational analysis. Adv Mater Res 154(155):1726–1738

21. El-Bahloul SA, El-Shourbagy HE, El-Bahloul AM, El-Midany TT (2018) Experimental and thermo-mechanical modeling optimization of thermal friction drilling for AISI 304 stainless steel. CIRP J Manuf Sci Technol 20:84–92

22. El-Bahloul SA, El-Shourbagy HE, El-Midany TT (2016) Effect of tool geometry, feed rate, and rotational speed of thermal friction drilling process on AISI 304 stainless steel. Mansoura Eng J 41(1):9–15

23. Krishna PVG, Kishore K, Satyanarayana VV (2010) Some investigations in friction drilling AA6351 using high speed steel tools. ARPN J Eng Appl Sci 5(3):11–15

24. Oezkaya E, Hannich S, Biermann D (2019) Development of a three-dimensional finite element method simulation model to predict modified flow drilling tool performance. Int J Mater Form 12:477–490

25. Bustillo A, Urbikain G, Perez JM, Pereira OM, de Lacalle LNL (2018) Smart optimization of a friction-drilling process based on boosting ensembles. J Manuf Sys 48:108–121

26. Krasauskas P (2011) Experimental and statistical investigation of thermo-mechanical friction drilling process. Mechanika 17(6):681–686

27. Boopathi M, Shankar S, Manikandakumar S, Ramesh R (2013) Experimental investigation of friction drilling on brass, aluminium and stainless steel. Procedia Eng 64:1219–1226

28. Demir Z, Ozek C (2013) Investigate the friction drilling of aluminium alloys according to the thermal conductivity. TEM J 2(1):93–101

29. Pantawane PD, Ahuja BB (2014) Parametric analysis and modelling of friction drilling process on AISI 1015. Int J Mechatronics Manuf Sys 7(1):60–79

30. Rao KH, Gopichand A, Kumar NP, Jitendra K (2017) Optimization of machining parameters in friction drilling process. Int J Mech Eng Technol 8(4):242–254

31. Dogru N, Ozler L, Tosun N (2013) Experimental and statistical evaluation on surface roughness and temperature in friction drilling. European conference in technology and society EuroTecS-2013 243-250.

32. Pantawane PD, Ahuja BB (2011) Experimental investigations and multi-objective optimization of friction drilling process on AISI 1015. Int J Appl Eng Res 2(2):448–461

33. Ku W, Hung C, Lee S, Chow H (2011) Optimization in thermal friction drilling for SUS 304 stainless steel. Int J Adv Manuf Technol 53:935–944

34. Biermann D, Walther F, Hannich S, Wittke P (2017) Front face flow drilling of lightweight cast materials. Procedia Eng 207:956–961

35. Dehghan S, Ismail MIS, Ariffin MKA, Baharudin BTHT (2018) Experimental investigation on friction drilling of titanium alloy. Eng Solid Mech 6(2):135–142

36. Somasundaram G, Boopathy SR (2010) Fabrication and friction drilling of aluminum silicon carbide metal matrix composite. Frontiers in Automobile and Mechanical Engineering -2010, Chennai 21–6.

37. Aslan F, Langlois L, Balan T (2019) Experimental analysis of the flow drill screw driving process. Int J Adv Manuf Technol 104:2377–2388

38. Sato YS, Kokawa H (2003) Friction stir welding (FSW) process. Weld Inter 17:852–855

39. Hynes NRJ, Kumar R, Sujana JAJ (2017) Optimum bushing length in thermal drilling of galvanized steel using artificial neural network coupled with genetic algorithm. Mater Technol 51(5):813–822

40. Shalamov PV, Kazantseva JV (2017) Thermal drilling with force-feed tool. Procedia Eng 206:985–990

41. Demir Z, Ozek C, Bal M (2018) An experimental investigation on bushing geometrical properties and density in thermal frictional drilling. Appl Sci 8/12:2658

42. Shalamov PV, Kulygina IA, Yaroslavova EN (2016) ANSYS software-based study of thermal drilling process. Procedia Eng 150:746–752

43. Fernández A, Lopez de Lacalle LN, Lamikiz A (2011) Friction drilling of stainless steels pipes. AIP Conf Proc 1315:1187

44. Vergara J, Damm S, Villanueva J, Godoy J-M, Tikal F (2001) Bush making by thermal flow drilling in copper and brass. Int J Manuf Sci Prod 4(2):103–111

45. Su K, Welo T, Wang J (2018) Improving friction drilling and joining through controlled material flow. Procedia Manuf 26:663–670

46. Urbikain G, Perez JM, Lopez de Lacalle LN, Andueza A (2018) Combination of friction drilling and form tapping processes on dissimilar materials for making nutless joints. Proc Ins Mech Eng Part B: J Eng Manuf 232(6):1007–1020

47. Lopez De Lacalle LN, Urbikain Pelayo G, Azkona I, Verbitchi V, Cojocaru R, Botila L, Ciuca C, Perianu I, Vlascici M (2018) Functional layers of aluminium alloy on steel made by alternative friction processes, for elements of metal structures. Adv Mater Res 1146:106–114

48. El-Bahloul SA (2019) Friction drilling of cast aluminum alloy A380 without significant petal formation and radial fracture. Int J Precision Eng Manuf 20:45–52

49. France JE, Davison JB, Kirby PA (1999) Strength and rotational stiffness of simple connections to tubular columns using flowdrill connectors. J Constrl Steel Res 50:15–34

50. Miller SF, Blau PJ, Shih AJ (2005) Microstructural alterations associated with friction drilling of steel, aluminum, and titanium. J Mater Eng Perform 14:647–653

51. Chow H, Lee S, Yang L (2008) Machining characteristic study of friction drilling on AISI 304 stainless steel. J Mater Process Technol 207:180–186

52. Kumar R, Hynes NRJ (2019) Influence of rotational speed on mechanical features of thermally drilled holes in dual-phase steel. Proc Inst Mech Eng Part B: J Eng Manuf 233(5):1614–1625

53. Wittke P, Liu Y, Biermann D, Walther F (2015) Influence of the production process on the deformation and fatigue performance of friction drilled internal threads in the aluminum alloy 6060. Mater Test 57(4):281–288

54. Wittke P, Walther F (2016) Cyclic deformation behavior of friction drilled internal threads in AlSi10Mg and AZ31 profiles. Procedia Struct Integr 2:3264–3271

55. Fernández Landeta J, Fernández Valdivielso A, López de Lacalle LN, Girot F, Pérez Pérez JM (2015) Wear of form taps in threading of steel cold forged parts. J Manuf Sci Eng 137(3):031002

56. Wittke P, Teschke M, Walther F (2018) Mechanical characterization of friction drilled internal threads in AZ91 profiles. Int J Adv Manuf Technol 99:3111–3122

57. Engbert T, Heymann T, Biermann D, Zabel A (2011) Flow drilling and thread forming of continuously reinforced aluminium extrusions. Proc Inst Mech Eng Part B: J Eng Manuf 225(3):398–407

58. Eliseev AA, Fortuna SV, Kolubaev EA, Kalashnikova TA (2017) Microstructure modification of 2024 aluminum alloy produced by friction drilling. Mater Sci Eng A. 691:121–125

59. Eliseev AA, Kalashnikova TA, Fortuna SV (2017) Microstructure evolution of AA3005 in friction drilling. AIP Conf Proc 1909: 020038

60. Eliseev AA, Kalashnikova TA, Fortuna SV (2017) Structure of AA5056 after friction drilling. AIP Conf Proc 1909:–020039

61. Fortuna SV, Kalashnikova TA, Kolubaev EA (2017) Structural and phase state evolution in friction drilling on AA2024. AIP Conf Proc 1909:020055

62. Bilgin MB, Gok K, Gok A (2017) Three-dimensional finite element model of friction drilling process in hot forming processes. Proc IMechE Part E: J Process Mech Eng 231(3):548–554

63. Qu J, Blau PJ (2008) A new model to calculate friction coefficients and shear stresses in thermal drilling. J Manuf Sci Eng 130:014502.

64. Li H, Chen L, Zhang C, Li Z (2018) An improved drilling force model in friction drilling AISI 321. IOP Conf. Series: J Phys: Conf. Series 1074:012147

65. Raju BP, Swamy MK (2012) Finite element simulation of a friction drilling process using deform-3D. Int J Eng Res Appl 2(6):716–721

66. Dehghan S, Ismail MIS, Ariffin MKA, Baharudin BTHT, Sulaiman S (2017) Numerical simulation on friction drilling of aluminum alloy. Mat.-wiss. u. Werkstofftech 48:241–248

67. Dehghan S, Ismail MISB, Souri E (2020) A thermo-mechanical finite element simulation model to analyze bushing formation and drilling tool for friction drilling of difficult-to-machine materials. J Manuf Process 57:1004–1018

68. Kumar R, Hynes NRJ (2018) Finite-element simulation and validation of material flow in thermal drilling process. J Brazilian Soc Mech Sci Eng 40:162

69. Freis AK (2013) Method of flow drill screwing parts, US patent #0195579 A1.

70. Skovron J, Mears L, Ulutan D, Detwiler D, Paolini D, Baeumler B, Claus L (2015) Characterization of flow drill screwdriving process parameters on joint quality. SAE Int J Mater Manf 8(1):35–44

71. Sonstabo JK, Holmstrom PH, Morin D, Langseth M (2015) Macroscopic strength and failure properties of flow-drill screw connections. J Mater Process Technol 222:1–12

72. Scholz CS, Kopp G, Friedrich HE (2016) Influence of corrosive conditions on the mechanical performance of flow drill screw joints between light metals. Mater Sci Forum 879:1725–1730

73. Huang C-P, Chen W-N, Sung S-J, Pan J (2018) Mechanical strength and failure mode of flow drill screw joints in coach-peel specimens of aluminum 6082-T6 sheets of different thicknesses and processing conditions. SAE Technol Paper 01:0116

74. Aslan F, Langlois L, Mangin P, Balan T (2018) Identification of drilling parameters during the flow drill screw driving process. Key Eng Mater 767:465–471

75. Meschut G, Janzen V, Olfermann T (2014) Innovative and highly productive joining technologies for multi-material lightweight car body structures. J Mater Eng Perform 23:1515–1523

76. Skovron JD, Rohan Prasad R, Ulutan D, Mears L, Detwiler D, Paolini D, Baeumler B, Claus L (2015) Effect of thermal assistance on the joint quality of Al6063-T5A during flow drill screwdriving. ASME J Manuf Sci Eng 137/5:051019

77. Nagel P, Meschut G (2017) Flow drill screwing of fibre-reinforced plastic-metal composites without a pilot hole. Weld World 61: 1057–1067

78. Szlosarek R, Karal T, Enzinger N, Hahne C, Meyer C, Berger A (2016) Experimental and numerical investigations on the punching failure of carbon fiber-reinforced plastics. Mater Test 58(7):617–621

79. Sonstabo JK, Morin D, Langseth M (2018) Static and dynamic testing and modelling of aluminium joints with flow-drill screw connections. Int J Impact Eng 115:58–75

80. Pan J, Chen W-N, Sung S-J, Su X, Friedman P (2018) Failure mode and fatigue behavior of flow drill screw joints in lap-shear specimens of aluminum 6082-T6 sheets of different thicknesses. SAE Technol Paper 01:1239

81. Milner JL, Gnaeupel-Herold T, Skovron JD (2016) Residual stresses in flow drill screwdriving of aluminum alloy sheets. Proceedings of the ASME 2016 International Manufacturing Science and Engineering Conference.

82. Grujicic M, Snipes J, Ramaswami S (2016) Process and product-performance modeling for mechanical fastening by flow drilling screws. Int J Struct Integr 7(3):370–396

83. Grujicic M, Snipes J, Ramaswami S (2017) Process modeling, joint virtual testing and construction of joint connectors for mechanical fastening by flow-drilling screws. Proc Inst Mech EngPart B: J Eng Manuf 231(6):1048–1061

84. Graf M, Sikora SP, Roider CS (2018) Macroscopic modeling of thin-walled aluminum-steel connections by flow drill screws. Thin-Walled Structures 130:286–296